



HAL
open science

Energy Metabolism Rewiring Precedes UVB-Induced Primary Skin Tumor Formation

Mohsen Hosseini, Léa Dousset, Walid Mahfouf, Martin Serrano-Sanchez, Isabelle Redonnet-Vernhet, Samir Mesli, Zeinab Kasraian, Emilie Obre, Marc Bonneu, Stephane Claverol, et al.

► **To cite this version:**

Mohsen Hosseini, Léa Dousset, Walid Mahfouf, Martin Serrano-Sanchez, Isabelle Redonnet-Vernhet, et al.. Energy Metabolism Rewiring Precedes UVB-Induced Primary Skin Tumor Formation. *Cell Reports*, 2018, 23 (12), pp.3621-3634. 10.1016/j.celrep.2018.05.060 . hal-02421137

HAL Id: hal-02421137

<https://cnrs.hal.science/hal-02421137>

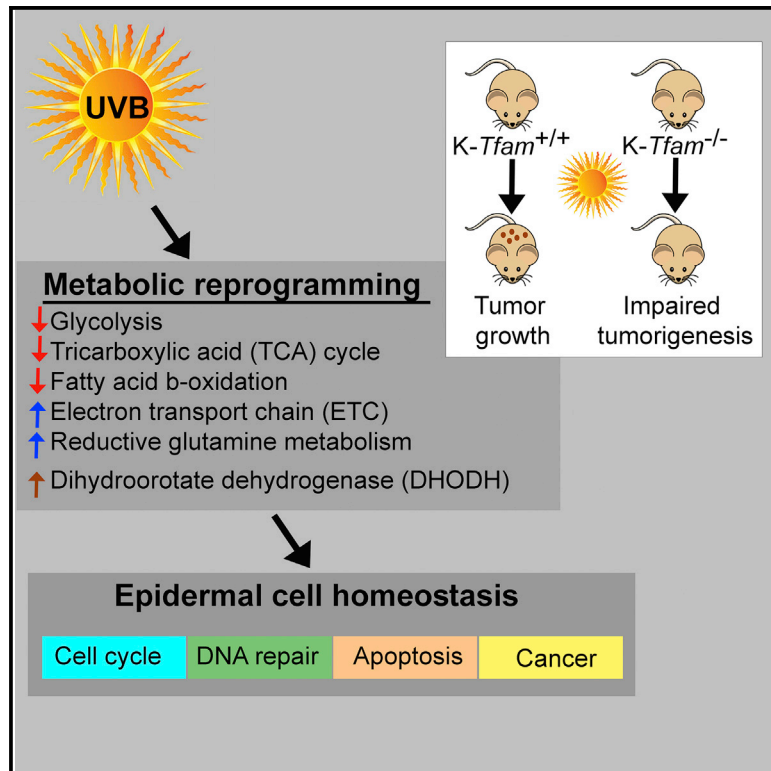
Submitted on 20 Dec 2019

HAL is a multi-disciplinary open access archive for the deposit and dissemination of scientific research documents, whether they are published or not. The documents may come from teaching and research institutions in France or abroad, or from public or private research centers.

L'archive ouverte pluridisciplinaire **HAL**, est destinée au dépôt et à la diffusion de documents scientifiques de niveau recherche, publiés ou non, émanant des établissements d'enseignement et de recherche français ou étrangers, des laboratoires publics ou privés.

Energy Metabolism Rewiring Precedes UVB-Induced Primary Skin Tumor Formation

Graphical Abstract



Authors

Mohsen Hosseini, Léa Dousset, Walid Mahfouf, ..., Anne-Karine Bouzier-Sore, Rodrigue Rossignol, Hamid Reza Rezvani

Correspondence

hamid-reza.rezvani@u-bordeaux.fr

In Brief

Hosseini et al. show that specific metabolic modifications occur at a very early stage of photocarcinogenesis. Those modifications ensure the coordination of ATP generation, persistent nucleotide biosynthesis and repair of DNA damage, which all play an important role in defining of epidermal cell fate.

Highlights

- Specific metabolic modifications precede UVB-induced primary tumor formation
- DHODH fuels mitochondrial respiration to coordinate DNA repair and ATP synthesis
- Respiration-linked nucleotide synthesis is necessary for primary skin tumor formation
- Impairment of ETC blocks neoplastic transformation of keratinocytes



Energy Metabolism Rewiring Precedes UVB-Induced Primary Skin Tumor Formation

Mohsen Hosseini,^{1,2} Léa Dousset,^{1,2} Walid Mahfouf,^{1,2} Martin Serrano-Sanchez,^{1,2} Isabelle Redonnet-Vernhet,^{3,4} Samir Mesli,³ Zeinab Kasraian,^{1,2} Emilie Obre,^{4,5} Marc Bonneau,⁶ Stephane Claverol,⁶ Marija Vlaski,⁷ Zoran Ivanovic,⁷ Walid Rachidi,⁸ Thierry Douki,⁸ Alain Taieb,^{1,2,9,10} Anne-Karine Bouzier-Sore,^{11,12} Rodrigue Rossignol,^{1,4,5,12} and Hamid Reza Rezvani^{1,2,9,13,*}

¹Inserm U 1035, BMGIC, 33076 Bordeaux, France

²Université de Bordeaux, 146 rue Léo Saignat, 33076 Bordeaux, France

³Service de Biochimie Métabolique, CHU de Bordeaux, France

⁴Inserm U1211 Maladies Rares: Génétique et Métabolisme (MRGM), Université de Bordeaux, Bordeaux, France

⁵CELLOMET, Centre de Génomique Fonctionnelle de Bordeaux, Université de Bordeaux, Bordeaux, France

⁶Plateforme de protéomique, Centre de Génomique Fonctionnelle de Bordeaux, Université de Bordeaux, Bordeaux, France

⁷Etablissement Français du Sang Aquitaine-Limousin, Université de Bordeaux, Bordeaux, France

⁸Nucleic Acids Lesions Laboratory, SCIB/INAC, CEA, Université Joseph Fourier- Grenoble, Grenoble, France

⁹Centre de Référence pour les Maladies Rares de la Peau, CHU de Bordeaux, France

¹⁰Service de Dermatologie Adulte et Pédiatrique, CHU de Bordeaux, France

¹¹Centre de Résonance Magnétique des Systèmes Biologiques, CNRS-Université Bordeaux, UMR 5536 Bordeaux, France

¹²These authors contributed equally

¹³Lead Contact

*Correspondence: hamid-reza.rezvani@u-bordeaux.fr

<https://doi.org/10.1016/j.celrep.2018.05.060>

SUMMARY

Although growing evidence indicates that bioenergetic metabolism plays an important role in the progression of tumorigenesis, little information is available on the contribution of reprogramming of energy metabolism in cancer initiation. By applying a quantitative proteomic approach and targeted metabolomics, we find that specific metabolic modifications precede primary skin tumor formation. Using a multistage model of ultraviolet B (UVB) radiation-induced skin cancer, we show that glycolysis, tricarboxylic acid (TCA) cycle, and fatty acid β -oxidation are decreased at a very early stage of photocarcinogenesis, while the distal part of the electron transport chain (ETC) is upregulated. Reductive glutamine metabolism and the activity of dihydroorotate dehydrogenase (DHODH) are both necessary for maintaining high ETC. Mice with decreased DHODH activity or impaired ETC failed to develop pre-malignant and malignant lesions. DHODH activity represents a major link between DNA repair efficiency and bioenergetic patterning during skin carcinogenesis.

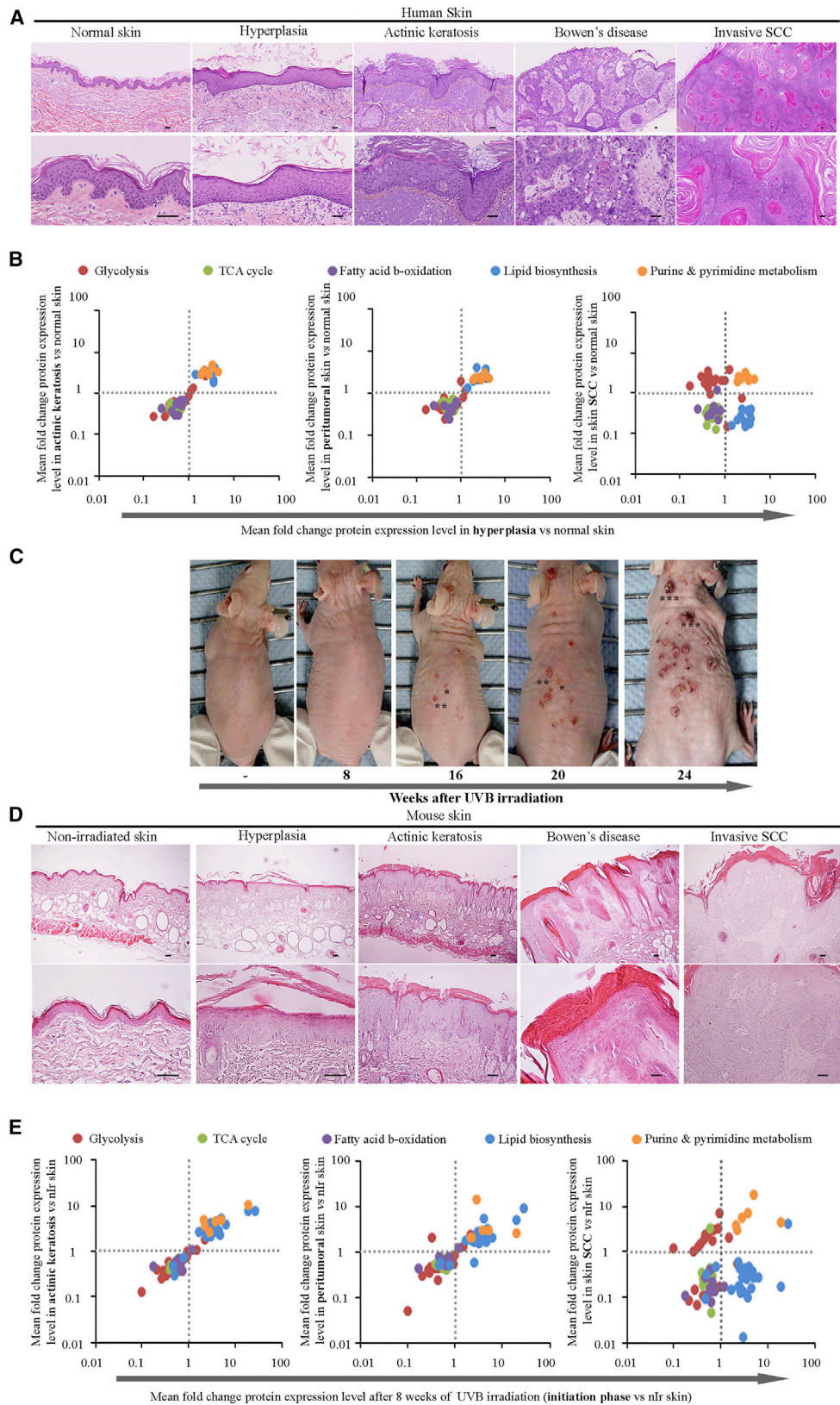
INTRODUCTION

The most common metabolic hallmark of malignant tumors (i.e., the “Warburg effect”) is their propensity to metabolize glucose to lactic acid at a high rate even in the presence of oxygen. Increased glucose uptake usually reflects an increased rate of glycolysis, with conversion of glucose to lactate and decreased utilization of pyruvate for mitochondrial oxidative phosphoryla-

tion (OXPHOS) (Liberti and Locasale, 2016; Zong et al., 2016). Since the seminal studies of Otto Warburg one century ago, biochemical research on cancer cell metabolism has revealed the highly metabolic plasticity of cancer cells. A large number of metabolic profiles have been discovered, from the highly glycolytic phenotype repeatedly observed on fast-growing cell lines (Vander Heiden et al., 2009; Ward and Thompson, 2012) to the completely opposite profile characterized by a higher dependency on OXPHOS, as found in metastasis (Porporato et al., 2014) or a subclass of diffuse B cell lymphomas (Caro et al., 2012). It is now widely accepted that OXPHOS and glycolysis cooperate to sustain the energy demands of cancer cells (Smolková et al., 2011; Ward and Thompson, 2012) and that cancer cells undergo metabolic reprogramming to maintain anabolism through various mechanisms including the deviation of glycolysis, Krebs cycle truncation, and OXPHOS redirection toward lipid and protein synthesis (Jose et al., 2011; Pavlova and Thompson, 2016). The critical role of mitochondria in carcinogenesis and gene regulation was further evidenced by recent studies on various oncometabolites produced by the tricarboxylic acid (TCA) cycle (Galluzzi et al., 2013; Ward and Thompson, 2012) and by the role of glutaminolysis, a biochemical pathway located in mitochondria (Villar et al., 2015). A better understanding of what determines tumor bioenergetics is also crucial for developing adapted metabolic therapies, as currently proposed for isocitrate dehydrogenase (IDH) 1 and 2 mutant tumors (Emadi et al., 2014; Seltzer et al., 2010).

Several genetic and biochemical mechanisms underlying the bioenergetic profiling of tumors have been discovered in the last decade (for review see Hosseini et al., 2017; Obre and Rossignol, 2015), but most of these findings were obtained on established tumors or on mouse models of cancer progression. Indeed, little attention has been given to the bioenergetic profiling of the cancer initiation phase and how it influences





(legend on next page)

further the bioenergetic behavior of tumors. In the present study, we investigated whether metabolic changes could be detected at the initial stages before typical pathological alterations of carcinogenesis occur, the impact of early metabolic changes in skin tumor formation, and whether these changes can be maintained throughout tumor development. Solar ultraviolet B (UVB) radiation is the primary environmental risk factor responsible for the induction of non-melanoma skin cancers (NMSC) including basal cell carcinomas (BCCs) and squamous cell carcinomas (SCCs), the most common types of human malignancies worldwide. An estimate 5.4 million cases of NMSCs were affecting 3.3 million patients among the US population in 2012 (Rogers et al., 2015). A major deleterious effect of UVB is the induction of well-defined structural alterations in DNA, which, in turn, trigger the DNA damage response (DDR) network. DDR involves sensing the damage and then transducing this signal to downstream effectors that elicit the appropriate responses including repair of DNA damage, cell-cycle delay, senescence, and/or apoptosis (Lagerwerf et al., 2011; Surova and Zhivotovskiy, 2013). The ultimate fate of cells with damaged DNA is, indeed, dependent on the type and extent of damage and DNA repair capacity (Branzei and Foiani, 2008; Surova and Zhivotovskiy, 2013). If not repaired or if misrepaired, UVB-induced DNA damage can ultimately contribute to the development of skin cancers.

In the current study, we show that chronic UVB irradiation results in energy metabolism reprogramming through activation of dihydroorotate dehydrogenase (DHODH) in the initial phase of carcinogenesis. In turn, upregulated DHODH and activated reductive glutamine metabolism work in concert to induce electron transport chain (ETC) activation and pyrimidine synthesis. Defects in these UVB-induced coordinated modifications, through inhibition of DHODH or ETC impairment, block neoplastic transformation of keratinocytes. These results demonstrate that metabolic changes precede tumor formation and that ETC activity plays a pivotal role in UVB-induced carcinogenesis.

RESULTS

Specific Reprogramming of the Metabolic Network Occurs at a Very Early Stage of Skin Carcinogenesis

It is now widely accepted that tumorigenesis is associated with altered metabolism (Hanahan and Weinberg, 2011). We

wondered whether metabolic reprogramming occurs during the initial phase of carcinogenesis. To this end, we first characterized the large-scale changes in the bioenergetic machinery of human skin at different stages of carcinogenesis using a quantitative label-free differential proteomic analysis of human skin hyperplasia (initial phase), actinic keratoses (AK, promotion phase), peritumoral skin, and squamous cell carcinomas (SCCs, progression stage) (Figures 1A and 1B; Table S1). A detail of the function of these proteins was obtained by performing a KEGG pathway analysis of the data using the String software (<https://www.ncbi.nlm.nih.gov/pubmed/25352553>). We found that the changes in the topology of the metabolic pathways involved in the energy metabolism were very similar between hyperplasia, AK, and peritumoral tissue. Interestingly, the metabolic profile of tumors was significantly different from that of pre-cancerous lesions. Of note, there was a dramatic downregulation of the enzymes involved in lipid biosynthesis and a substantial upregulation of several enzymes involved in glycolysis (Figure 1B; Table S1). Therefore, it was considered likely that specific metabolic modifications, of which some persist throughout tumor development, occur at a very early stage of skin carcinogenesis. An *in vivo* model was then used to examine the mechanisms underlying those early metabolic changes. To this end, SKH-1 hairless mice, which closely mimic photocarcinogenesis in humans (DiGiovanni, 1992), were exposed to chronic UVB irradiation. As seen in Figures 1C and 1D, different stages (initiation, promotion, and progression) of skin carcinogenesis were easily evidenced at different times after chronic UVB irradiation. Indeed, during the first few weeks of chronic UVB irradiation, mice presented moderate hyperplasia and no papillomatosis. Mild nuclear atypia was observed within basal keratinocytes. These modifications were subtle and were only identified histologically. Mice started to develop pre-malignant AK-like lesions (promotion stage) after 13 weeks of chronic irradiation. At that time, greater cellular atypia and epidermal hyperplasia were also observed. Of these AK, some progressed into small keratotic and large ulcerated tumors resembling human SCCs (progression stage), with the potential for metastatic spread after 20 weeks of UVB irradiation (Figures 1C and 1D). We then compared the metabolic changes described by the proteomic analysis of skin hyperplasia, AK, peritumoral skin, and full-blown SCC (Figure 1E; Table S2). The changes in the topology of the metabolic pathways involved in the energy metabolism at

Figure 1. Metabolic Profiles Are Very Similar among Epidermal Hyperplasia, Actinic Keratosis, and Peritumoral Tissue

- (A) Histopathological alterations in the human skin at different stages of carcinogenesis were evaluated with H&E staining. Scale bars, 50 μ m.
- (B) Skin biopsies were subjected to proteomic analysis. Scatterplots show comparison of fold change of protein expression levels between hyperplasia and actinic keratosis (left), hyperplasia and peritumoral tissue (middle), and hyperplasia and full-blown SCC (right). Each color dot represents an individual protein. N = 20 samples per group. Red, green, purple, blue, and orange points indicate the proteins involved in glycolysis, TCA cycle, fatty acid β -oxidation, lipid biosynthesis, and purine and pyrimidine metabolism, respectively.
- (C) SKH-1 hairless mice were exposed to 150 mJ/cm², corresponding to one minimal erythemal dose, three times per week. During the first few weeks of chronic UVB irradiation (initial phase), mice did not display macroscopic anomalies. Precursor lesions known as actinic keratoses (AK, promotion stage) started to appear after 13 weeks of chronic irradiation. Of these AK, some progressed into squamous cell carcinoma (SCC), *in situ* (Bowen's disease), and invasive SCC. Examples of clinical lesions are shown: *actinic keratosis, **Bowen's disease, ***invasive SCC.
- (D) Histological analysis at initial phase indicates moderate hyperplasia and no papillomatosis. Mild nuclear atypia is also observed within basal keratinocytes. At promotion stage, histological analysis reveals greater epidermal hyperplasia consisting of keratinocytes manifesting atypical nuclei that are enlarged, irregular, and hyperchromatic. Scale bars, 50 μ m.
- (E) Skin biopsies of irradiated and non-irradiated mice were subjected to proteomic analysis. Scatterplots show comparison of fold change of protein expression levels between indicated groups. Each color dot represents an individual protein. N = 12 samples per group

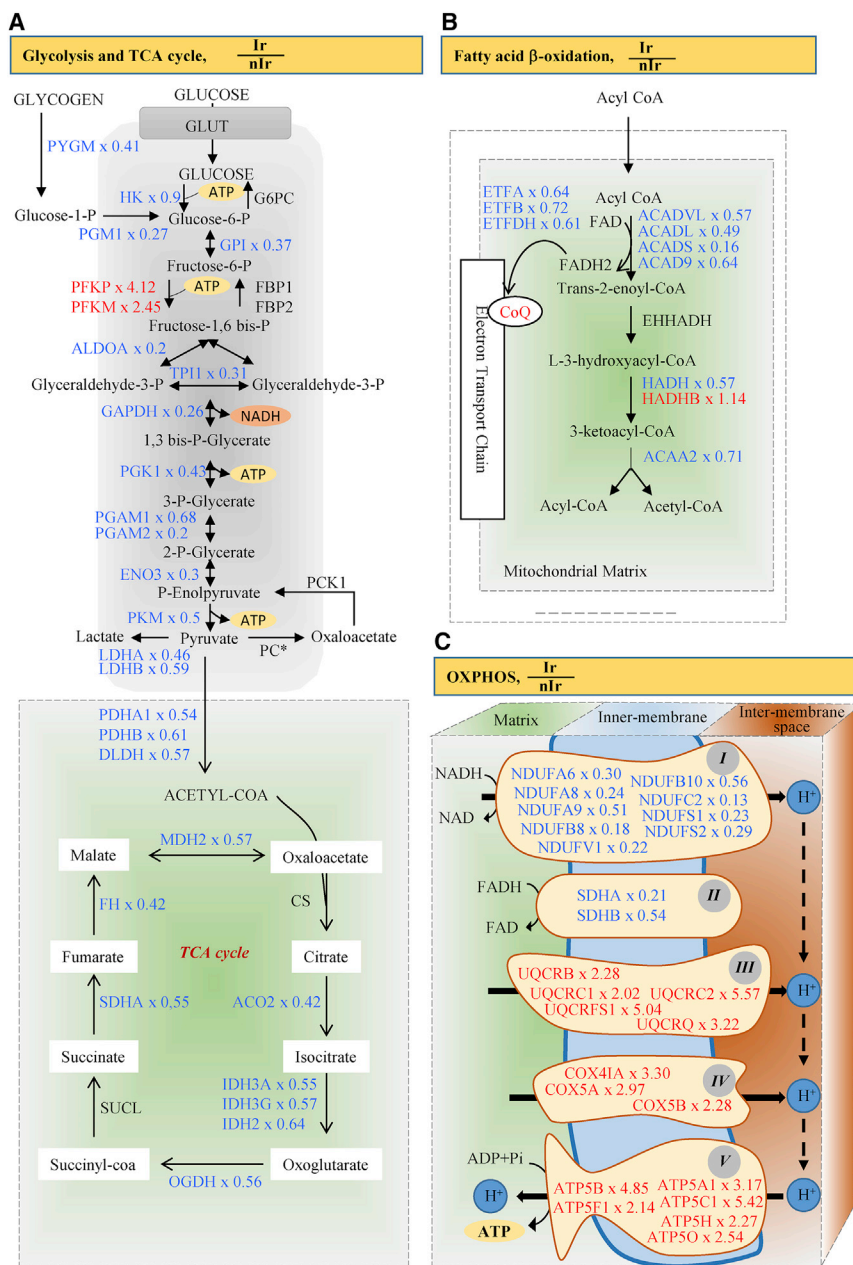


Figure 2. UVB Irradiation Downregulates the Majority of Proteins Involved in Glycolysis, TCA Cycle, and Fatty Acid β -Oxidation

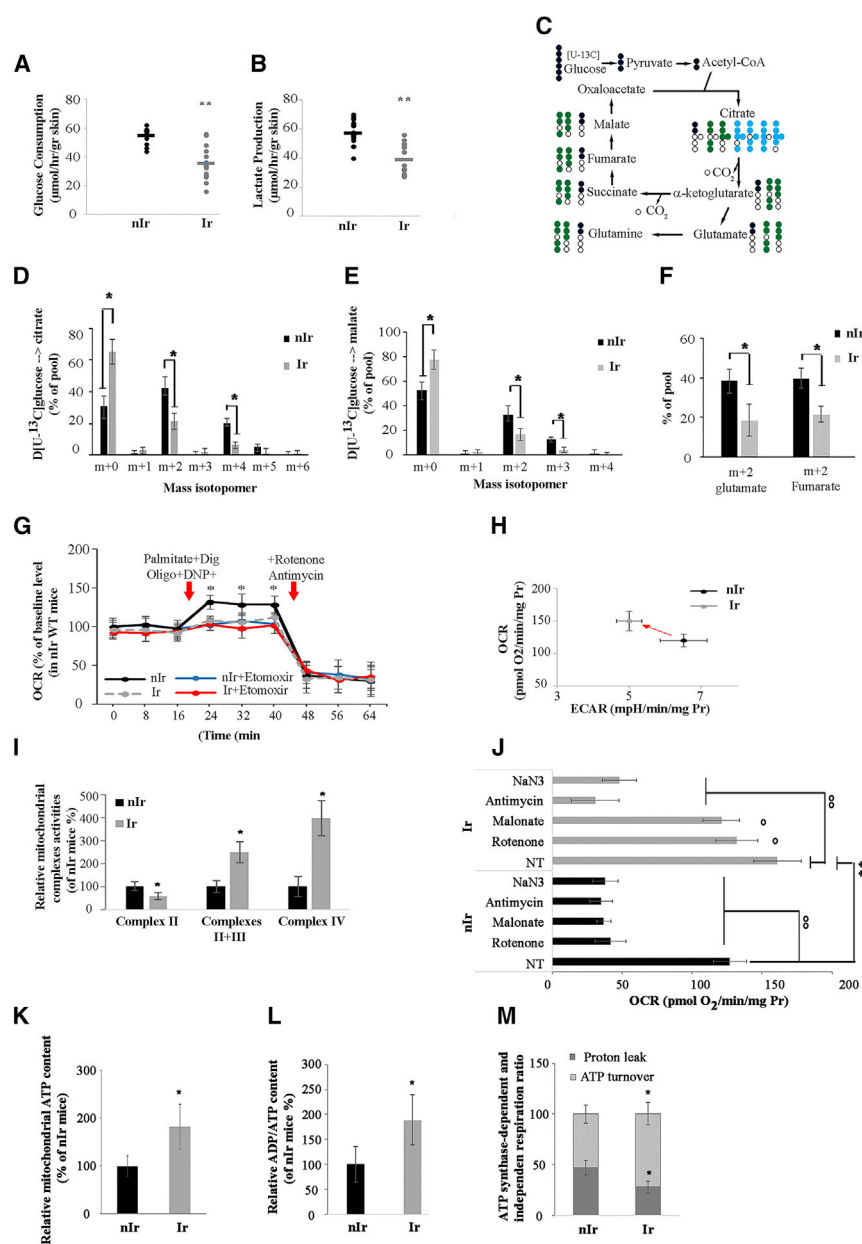
Proteomic analysis was used to investigate the effects of chronic UVB irradiation on the profile expression of several proteins in skin biopsies of SKH-1 mice. To this end, skin biopsies of mice irradiated for 2 months (Ir) and non-irradiated (nIr) counterparts were subjected to proteomic analysis. The quantity of each protein involved in glycolysis, TCA cycle (A), fatty acid β -oxidation (B), and electron transport chain (ETC) (C) was compared between Ir and nIr groups and the results are expressed as mean fold change of expression of each protein. N = 8 mice per group. ACAD, acyl-CoA dehydrogenase; ACAD(VL, L and S), very long-, long-, and short-chain-specific acyl-CoA dehydrogenase; ACO, aconitate hydratase; ATP5, ATP synthase; COX, cytochrome C oxidase; CS, citrate synthase; ENO3, beta-enolase; ETF(A and B), electron transfer flavoprotein (alpha and beta); ETFDH, ETF-ubiquinone oxidoreductase; FH, fumarate hydratase; GPI, glucose-6-phosphate isomerase; HADH, hydroxyacyl-CoA dehydrogenase/3-ketoacyl-CoA thiolase/enoyl-CoA hydratase; HK, hexokinase; IDH, isocitrate dehydrogenase; LDH, L-lactate dehydrogenase; MDH, malate dehydrogenase; NDUF, NADH dehydrogenase (ubiquinone); OGDH, 2-oxoglutarate dehydrogenase; PDH, pyruvate dehydrogenase; PFK(P, M, and L), 6-phosphofructokinase (platelet, muscle, and liver type); PGAM, phosphoglycerate mutase; PGK, phosphoglycerate kinase; PGM, phosphoglucomutase; PKM, pyruvate kinase; PYGM, glycogen phosphorylase, muscle form; SDH, succinate dehydrogenase; SUCL, succinyl-CoA ligase; TPI, triosephosphate isomerase; UQCR, ubiquinol-cytochrome C reductase.

formed. Results revealed lower glucose consumption and lactate production in irradiated skin than in non-irradiated skin (Figures 3A and 3B). To determine the effects of UVB irradiation on the metabolic fates of glucose, [U - ^{13}C]-labeled glucose (here U indicates uniformly labeled) was injected intraperitoneally (i.p.) into two groups of mice, and ^{13}C enrichment of intracellular metabolites was measured by mass spectrometry. In non-irradiated cells, most citrate molecules (>60%) contained glucose-derived ^{13}C (Figures 3C and 3D). Citrate m+2 (citrate containing two additional mass units from ^{13}C) results from oxidative decarboxylation of glucose-derived pyruvate by pyruvate dehydrogenase (PDH) to form [1,2- ^{13}C]acetyl-coA, followed by condensation with an unlabeled oxaloacetate (OAA). Processing of citrate m+2 around one turn of the TCA produces citrate m+4 (Figure 3C). In irradiated skin, most citrate contained no glucose carbon (m+0), indicating significant reduction of PDH contribution to acetyl-CoA (Figure 3C). Malate, fumarate and glutamate m+2 were also decreased in irradiated skin (Figures 3E and 3F).

different stages of photocarcinogenesis were very similar to those found in human samples.

Focusing on metabolic changes of mouse skin exposed to chronic UVB irradiation for 8 weeks (initial stage of carcinogenesis), the majority of proteins involved in the glycolysis, TCA cycle, and fatty acid β -oxidation were shown to be significantly decreased, respectively from 50% to 80%, from 36% to 58%, and from 28% to 84%, in irradiated skin. On the contrary, irradiation increased proteins involved in the distal part of the electron transport chain (ETC) with overexpression values ranging from 2.02- to 5.57-fold (Figures 1E and 2; Table S2).

To further verify the effects of chronic UVB irradiation on energy metabolism, biochemical functional analyses were per-



Results are presented as means ± SD. N = 15 mice (A, B, and G–M) and 6 mice (D–F) for each group. *p < 0.05 and ** < 0.01 for irradiated versus non-irradiated mice. O p < 0.05 and OO p < 0.01 for treated versus non-treated irradiated mice. Dig, digitonin; Oligo, oligomycin; DNP, 2,4-dinitrophenol.

To assess the effects of UVB irradiation on fatty acid β-oxidation, we measured the respiratory capacity of digitonin-permeabilized skin in the presence of carnityl-palmitate as energy substrate. Irradiated skin was unable to trigger a substantial switch to fatty acid oxidation when shifted from no-glucose to palmitate-supplemented medium, reflected by a 1.40-fold lower basal oxygen consumption rates (OCR) burst than that in non-irradiated skin (Figure 3G).

To evaluate the OXPHOS activity following irradiation, basal OCR was first measured. Results indicated that basal OCR obtained in complete media was higher in irradiated skin than in

Figure 3. UVB Irradiation Results in Down-regulation of Glycolysis, TCA Cycle, and Fatty Acid β-Oxidation and Overactivation of Distal Part of OXPHOS

SKH-1 mice exposed to chronic UVB irradiation for 8 weeks.

(A and B) The glucose uptake and lactate production by skin biopsies taken from irradiated and non-irradiated mice were measured. Skin biopsies of irradiated mice consume less glucose (A) and produce less lactate (B).

(C) Schematic depicting glucose carbon flow into TCA metabolites. Black color represents labeled carbon on 1st TCA cycle, green color represents labeled carbon on 2nd TCA cycle, and blue color represents labeled carbon on 3rd TCA cycle (C). (D–F) Mass isotopomer analysis of citrate (D), malate (E), and glutamate and fumarate (F) in skin of irradiated and non-irradiated mice received intraperitoneally [U-¹³C] labeled glucose.

(G) The respiratory capacity of skin biopsies taken from irradiated and non-irradiated skin in the presence of carnityl-palmitate as energy substrate were measured. Kinetics of basal oxygen consumption rate (OCR) response to palmitate indicates a significant decrease in fatty acid oxidation in irradiated skin biopsies. Etomoxir inhibits fatty acid beta-oxidation by binding to carnitine palmitoyltransferase and preventing entry of fatty acids into the mitochondria.

(H) OCR and extracellular acidification rate (ECAR) were determined using Seahorse XF24 Extracellular Flux Analyzer in irradiated and non-irradiated skin. UVB irradiation is associated with an increased basal OCR and a decreased extracellular acidification rate (ECAR).

(I) The maximal activities of mitochondrial complexes II, III, and IV were measured in irradiated and non-irradiated mice. UVB irradiation results in over-activation of complexes III and IV.

(J) Basal OCR level was measured in skin samples treated with mentioned inhibitors of mitochondrial complexes. Increased OCR in UVB-irradiated skin are blocked when samples are treated with inhibitors of complexes III and IV (i.e., antimycin and sodium azide).

(K–M) UVB irradiation results in an increased mitochondrial ATP content (K), elevation of ADP/ATP ratio (L), and increased oligomycin-sensitive respiration (the portion of respiration used for ATP turnover) (M).

non-irradiated skin (Figure 3H). The discrepancy between Figures 3G and 3H on the basal OCR in irradiated skin may be explained by the difference in the medium used. In fact, to measure fatty acid oxidation capacity in Figure 3G, skin were placed in minimal medium in which carnityl-palmitate was added afterward. On the contrary, to measure OXPHOS activity, skin was placed in complete medium (see the Experimental Procedures for details). To further determine the effect of chronic UVB irradiation on OXPHOS activity and capacity, we first evaluated the maximal activities of the different enzyme complexes. While the activity of complex II was significantly diminished following

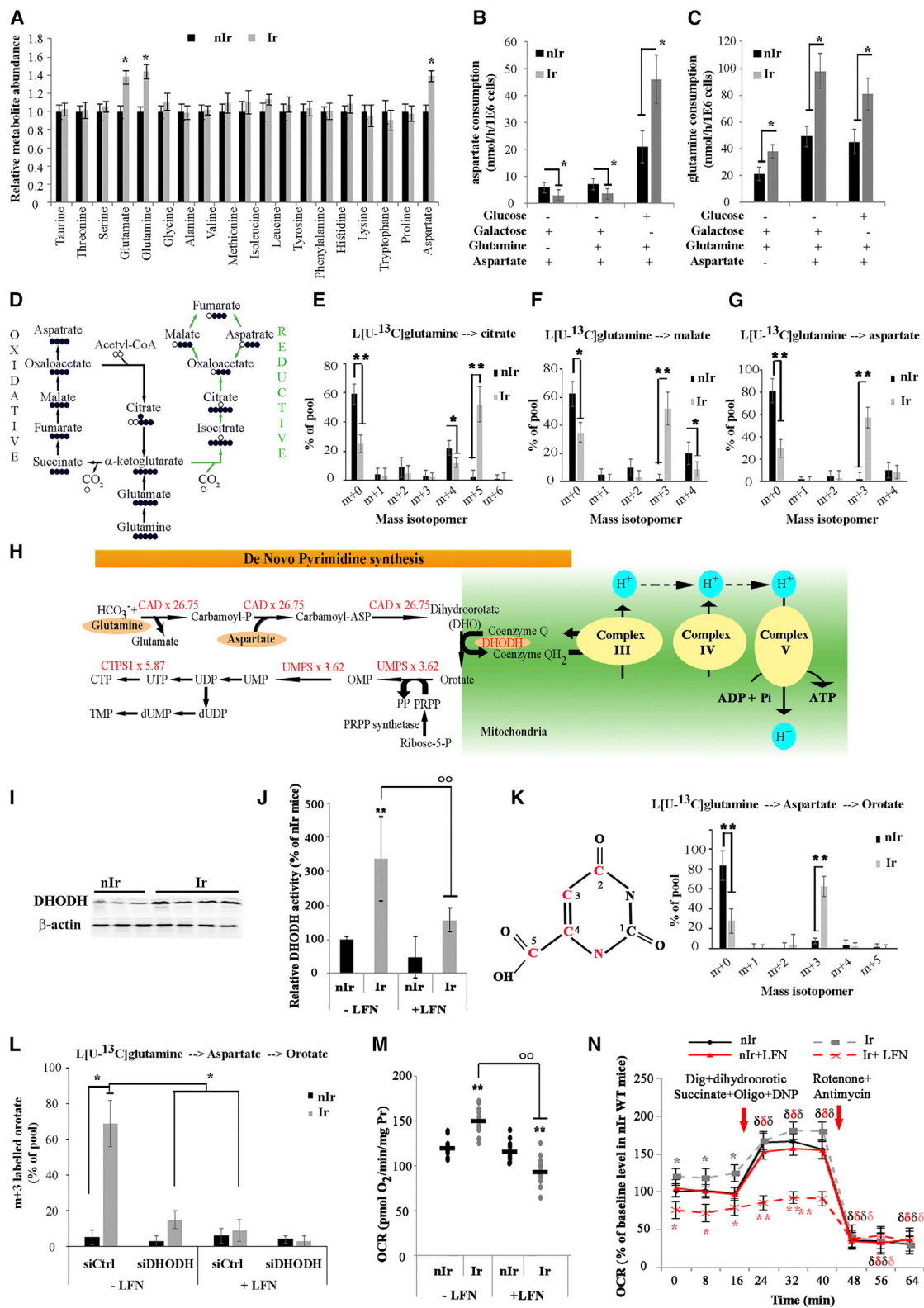


Figure 4. UVB Irradiation Triggers Reductive Glutamine Metabolism and Activation of DHODH that Drive Increased ETC Activation

(A) Relative abundance of indicated amino acids in skin biopsies of mice irradiated for 2 months (Ir) and non-irradiated (nlr) counterparts were quantified. All measurements are relative to non-irradiated skin.

(legend continued on next page)

irradiation, the activities of complexes II+III and IV were markedly increased (Figure 3I), suggesting a specific increased utilization of the distal part of ETC after UVB irradiation. This is in agreement with inhibitor titration studies showing that rotenone and malonate only decreased moderately the baseline OCR level in irradiated skin, by 18% and 25%, respectively, while antimycin and NaN₃ reduced it by ~81% and ~70% (Figure 3J). These results suggested a major role for complexes III and IV in elevated OCR in irradiated skin and a potential increased fueling of the respiratory chain between complex II and complex III in irradiated skin samples. We then verified that such increase in mitochondrial respiration was coupled to an increase in mitochondrial ATP content (Figure 3K). The ADP/ATP ratio in irradiated skin was also higher than in non-irradiated mice, suggesting a higher cellular energy demand in irradiated skin (Figure 3L). Finally, the proportion of respiration used to produce ATP (the oligomycin-sensitive respiration) was increased in irradiated skin compared with non-irradiated skin (Figure 3M).

Consistent with the topology obtained by proteomic analysis, biochemical functional analyses revealed that UVB irradiation results in (1) downregulation of glycolysis, TCA cycle, and fatty acid β -oxidation, and (2) increased distal part of OXPHOS. Furthermore, these results indicate that a specific mode of electron-fueling to the ETC occurs following chronic irradiation.

Increased ETC Activity in Chronic UVB Irradiated Skin Is Related to the Activity of DHODH and Reductive Glutamine Metabolism

Downregulation of glycolysis, TCA cycle, and fatty acid β -oxidation, despite maintenance of high OXPHOS, raised an important question: which carbon source is exploited in irradiated skin for maintaining OXPHOS. To answer this question, quantitative metabolomics analysis of intracellular free amino acids was performed. Among different amino acids, the abundance of glutamate, glutamine, and aspartate were respectively 1.37-, 1.45-, and 1.39-fold higher in irradiated samples than in non-irradiated

cells (Figure 4A). To examine whether glutamine or aspartate flux could provide an insight into biochemical processes occurring within the irradiated cells, we measured the consumption rate of glutamine and aspartate. Results revealed higher glutamine consumption and lower aspartate consumption in irradiated skin than in non-irradiated samples when cells were placed in medium supplemented with glucose, glutamine, and aspartate or in medium containing glutamine and aspartate. On the contrary, in the medium without glucose and glutamine, irradiated cells had a higher consumption of aspartate than non-irradiated cells (Figures 4B and 4C). To further define the metabolic fates of glutamine, cells isolated from irradiated and non-irradiated mice were cultured in medium supplemented with L[U-¹³C]glutamine. While non-irradiated cells used glutamine through oxidative glutamine metabolism, resulting in formation of citrate and malate m+4 (Figures 4D and 4F), irradiated cells produced mainly citrate m+5 and malate m+3 through reductive carboxylation of glutamine-derived α -ketoglutarate (Figures 4D–4F). Moreover, irradiated cells contained abundant aspartate m+3, which was essentially absent from non-irradiated cells (Figure 4G), indicating that irradiated cells used preferentially reductive glutamine metabolism to provide aspartate.

To understand the link between the stimulation of distal part of ETC and increased consumption of glutamine following irradiation, we performed a search on the proteomic data. We found that the enzymes involved in pyrimidine synthesis, in which glutamine and aspartate are used as key anaplerotic substrates, were markedly increased in irradiated skin compared to non-irradiated skin (Figure 4H). Because DHODH is the only mitochondrial enzyme of this pathway that converts dihydroorotate to orotate coupled with the reduction of ubiquinone to ubiquinol, we wondered whether DHODH is the link between increased glutamine and oxygen consumption in irradiated cells. To test this hypothesis, we first measured the expression and activity of DHODH in irradiated and non-irradiated mice. DHODH protein expression level as well as enzyme activity were markedly

(B and C) Skin samples taken from irradiated and non-irradiated mice were incubated DMEM medium supplemented with glucose, glutamine, and/or aspartate for 5 hr. Measurement of aspartate (B) and glutamine (C) uptake indicated irradiated skin consume less aspartate and more glutamine in the presence of glucose, glutamine, and/or aspartate.

(D) Schematic depicting carbon atom (circles) transitions in oxidative (black arrows) and reductive (green arrows) glutamine metabolism using [U-¹³C] glutamine. (E–G) Mass isotopologue analysis of citrate (E), malate (F), and aspartate (G) in non-irradiated and irradiated cells cultured with [U-¹³C] glutamine and unlabeled glucose for 5 hr.

(H) Skin biopsies of mice nlr and lr mice were subjected to proteomic analysis. The quantity of each protein involved in *de novo* pyrimidine synthesis was compared between nlr and lr groups, and the results are expressed as mean fold change of expression of each protein.

(I) The protein expression level of DHODH was determined by western blot. β -actin was used as a loading control. UVB irradiation leads to upregulation of DHODH protein level.

(J) The relative DHODH activity in irradiated and non-irradiated skin was measured. Increased DHODH activity in UVB-irradiated skin samples is blocked following treatment of mice with leflunomide (LFN), an inhibitor of DHODH.

(K) Isotopomer distribution of orotate from non-irradiated and irradiated cells cultured with [U-¹³C]glutamine and unlabeled glucose for 5 hr. Left: atoms of orotate that are derived from aspartate are shown in red.

(L) Percentage of orotate m+3 isotopologue was compared between siCtrl- and siDHODH-transfected cells cultured for 5 hr with L[U-¹³C] glutamine + unlabeled glucose \pm LFN.

(M and N) Chronic UVB-irradiated and non-irradiated mice received intraperitoneal injection of placebo or LFN 2 hr prior to sacrifice. The OCR of skin biopsies was determined and indicated that LFN treatment blocks UVB exposure-mediated increased basal OCR in mouse skin (M). Kinetics of OCR response of skin biopsies to dihydroorotic acid were assessed. UVB-irradiated skin samples display increased OCR level upon supplementation with 10 mM dihydroorotic acid (N). Results are presented as means \pm SD. N = 6 [(A–C, E–G, K)], 4 [L] and 12 [(I–J, M–N)] mice per group. *p < 0.05 and ** < 0.01 for irradiated versus non-irradiated mice. δ < 0.01 for treated samples versus corresponding basal OCR level. $^{\circ\circ}$ p < 0.01 for LFN-treated irradiated mice versus placebo-treated irradiated mice. PRPP, phosphoribosylpyrophosphate; CAD, carbamoyl-phosphate synthetase 2, aspartate transcarbamylase, and dihydroorotase; CTPS1, CTP synthase; DHODH, DHO dehydrogenase; OMP, orotidine 5'-monophosphate; UMPS, uridine 5'-monophosphate synthase.

upregulated in irradiated skin (Figures 4I and 4J). To examine whether glutamine-derived aspartate contributes to pyrimidine synthesis, epidermal cells isolated from non-irradiated and irradiated mice were incubated for 5 hr in the medium supplemented with labeled [U-¹³C] glutamine. Results indicated that in contrast to non-irradiated skin, irradiated cells contained abundant labeled m+3 orotate, a central intermediate of pyrimidine synthesis (Figure 4K). To confirm that the contribution of glutamine-derived aspartate to orotate synthesis is dependent on DHODH activity, epidermal cells were transfected with siDHODH, prior to culturing in the medium supplemented with labeled [U-¹³C] glutamine ± leflunomide (LFN, 50 μM), a potent but non-specific inhibitor of DHODH and a FDA-approved drug for the treatment of rheumatoid arthritis. Results indicated that the entry of aspartate-derived ¹³C into orotate was abolished in both LFN-treated and siDHODH-transfected cells (Figure 4L).

We then investigated the link between DHODH and ETC activation. To examine whether increased oxygen consumption in irradiated skin was dependent on DHODH activity, one group of chronic UVB-irradiated mice received intraperitoneally LFN (20 mg/kg/day), 2 hr prior to sacrifice. Baseline OCR levels were dramatically decreased when irradiated mice received LFN (Figure 4M). In contrast, a significant increase in ETC utilization was noted when irradiated skin was supplemented with dihydroorotic acid (Figures 4N and S1). To further confirm the effect of DHODH on oxygen consumption, OCR were measured in siDHODH-transfected keratinocytes isolated from irradiated or non-irradiated skin. DHODH downregulation led to a significant decrease in basal OCR levels (Figure S2A).

To survey the effect of DHODH on the observed increase in complex III activity, the activities of complexes II+III were measured in siDHODH-transfected keratinocytes isolated from irradiated or non-irradiated skin as well as in the presence of LFN (50 μM). Inhibition or downregulation of DHODH blocked over-activation of complexes II+III in UVB-irradiated skin (Figure S2B). Finally, to examine whether glutamine, aspartate, and DHODH are needed for maintenance of the high OXPHOS in irradiated skin, keratinocytes isolated from irradiated or non-irradiated skin were transfected with siDHODH or siCtrl. These cells were then incubated in DMEM medium without glucose, glutamine, and aspartate for 2 hr. Basal OCR were then measured following addition of glucose (5 mM) ± glutamine (5 mM) and aspartate (5 mM) in medium. Results indicated that basal OCR obtained in media supplemented with glutamine and aspartate was higher in irradiated skin than in non-irradiated skin (Figure S2C). Furthermore, the upregulation of OCR in irradiated cells was dependent on the DHODH expression (Figure S2C).

Overall, our results show that reductive glutamine metabolism and DHODH activity are both necessary to maintain high OXPHOS in irradiated cells.

Inhibition of DHODH Activity or Global Downregulation of ETC Results in Hypersensitivity to UVB Exposure

To evaluate the impact of DHODH upregulation and ETC activation on UVB-induced skin carcinogenesis, we used the following approaches: (1) the inhibition of DHODH using LFN, and (2) a mouse model of inducible *Tfam* knockout targeted to keratinocytes (K14-Cre-ER^{T2}/*Tfam*^{fllox/fllox}). The *Tfam* knockout model

was chosen because TFAM is the main regulator of mtDNA transcription and consequently of the mitochondrial genes encoding ETC subunits (Campbell et al., 2012; Kang et al., 2007). As seen in Figure 5A, while the expression of mitochondrial-encoded NADH dehydrogenase 1 (MT-ND1), cytochrome c oxidase 1 (MT-CO1), and ATP synthase 6 (MT-ATP6) proteins were significantly reduced in *Tfam*-ablated mice, the expression of nuclear-encoded mitochondrial complex 1 subunit NDUF8, II subunit SDHB, III subunit UQCRC2, and V subunit ATP5A did not change. Moreover, there was a marked reduction in DHODH expression and activity in the skin of *Tfam*-ablated mice (Figures 5A and 5B), suggesting a complex link between OXPHOS genes and DHODH expression. To further explore this relationship, keratinocytes were treated with pharmacological activators of mitochondrial biogenesis (AICAR and resveratrol) or inducers of the retrograde response using OXPHOS blockers (Rotenone, antimycin, DNP). Assessment of the DHODH expression and activity revealed that DHODH was a part of a general program of mitochondrial biogenesis (Figures S3A and S3B). We developed an inducible mouse model because mice with epidermal *Tfam* ablation (K14-Cre/*Tfam*^{fllox/fllox}) have been shown to have a short lifespan owing to malnutrition (insufficient milk intake) (Baris et al., 2011). To avoid the effect on nutrition, *Tfam* was ablated by topical skin application of tamoxifen in keratinocytes of K14-Cre-ER^{T2}/*Tfam*^{fllox/fllox} mice, hereinafter called K-*Tfam*^{-/-}. As controls, we used tamoxifen-treated K14-Cre-ER^{T2} mice, hereinafter referred to as K-*Tfam*^{+/+}. Because there were no meaningful differences in outcome between mice receiving LFN and K-*Tfam*^{-/-} mice, hereinafter only the results of K-*Tfam*^{+/+} and K-*Tfam*^{-/-} are shown.

We first monitored LFN-treated and K-*Tfam*^{-/-} mice and their control counterparts during the first 4 months of life. The mice developed normally and histological analysis of skin revealed a normal epidermis with no obvious abnormality in epidermal differentiation or proliferation (Figure 5C), in contrast with impaired epidermal differentiation noted in the epidermal constitutionally deleted *Tfam* mouse (Hamanaka et al., 2013). These mice were then exposed to chronic UVB irradiation. The LFN-treated and K-*Tfam*^{-/-} mice exhibited a UVB-related phenotype very early (Figure 6A). Indeed, 9 out of the 15 K-*Tfam*^{-/-} and 8 out of the 12 LFN-treated mice exhibited thick squamous hyperkeratotic plaques 12 weeks after UVB irradiation (Figure 6B). In 2 out of the 9 K-*Tfam*^{-/-} mice, stratum corneum sloughing of a large part of the dorsal skin was also noticed. Twenty weeks after chronic UVB irradiation, all of these mice presented desquamative features with a hyperkeratotic epidermis (Figure 6B). However, none of them developed AK and/or keratotic tumors up to 30 weeks after irradiation (Figures 6B and 6C). In contrast, none of the control mice had any obvious abnormality up to week 12 after irradiation, and 8 out of the 15 K-*Tfam*^{+/+} exhibited at least one AK lesion at 18 weeks (Figures 6A–6D). To further determine that hyperkeratotic plaques did not have tumorigenic potential, one group of mice was kept under observation (without further UVB exposure) following 20 weeks of chronic UVB irradiation. While tumors developed on the back of K-*Tfam*^{+/+} mice and new tumors continued to appear over time (Figures 6E and 6F), hyperkeratotic plaques healed, and no tumors were detected on K-*Tfam*^{-/-} mice (Figures 6E and 6G).

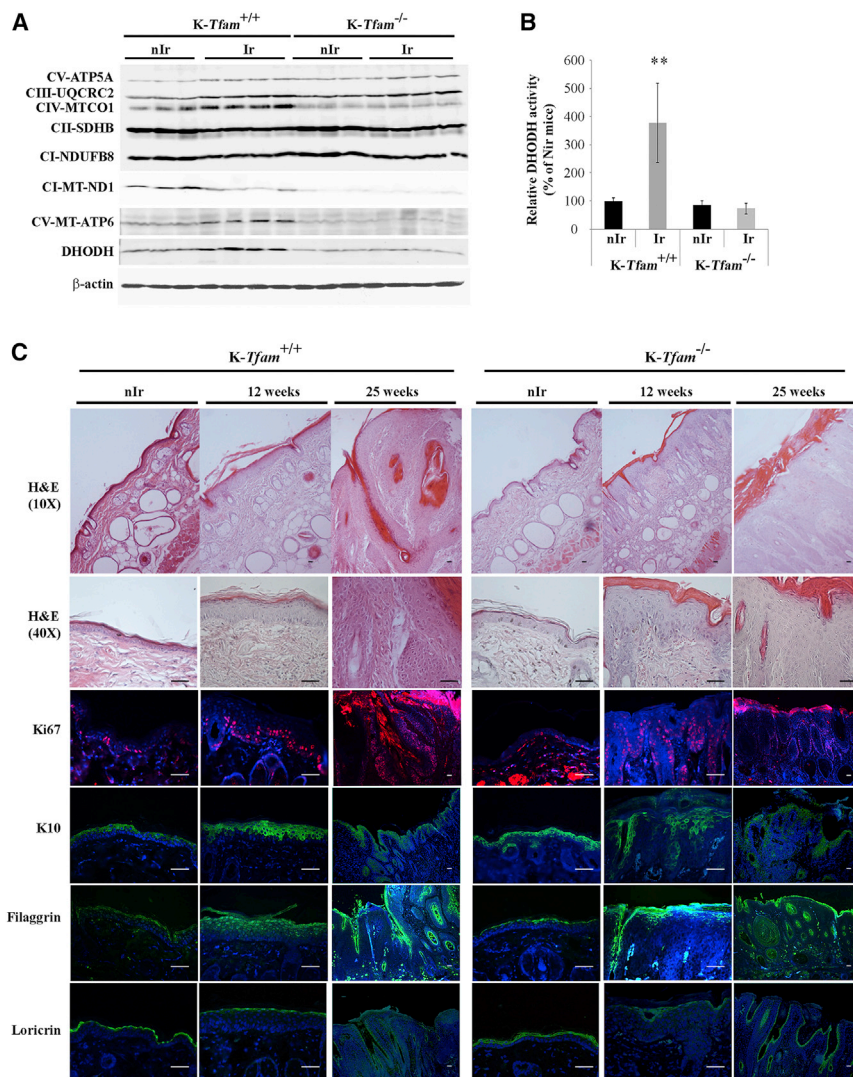


Figure 5. UVB Exposure-Mediated DHODH Activation Is Blocked upon Epidermal Ablation of Mitochondrial Transcription Factor A (*Tfam*)

(A) Total protein extracts of skin biopsies were assessed for expression of mitochondrial-encoded enzymes and DHODH by western blot. β-Actin was used as a loading control.

(B) Epidermal ablation of *Tfam* results in down-regulation of DHODH activity. Results are presented as means ± SD.

(C) *Tfam*-ablated mice (*K-Tfam*^{-/-}) and their control counterparts (*K-Tfam*^{+/+}) were subjected to chronic UVB irradiation and skin biopsies were taken at indicated times. Histopathology of epidermis was evaluated with H&E staining. Differentiation status of epidermis was assessed using immunofluorescence staining of K10, filaggrin, and loricrin. Proliferation was evaluated by Ki67 immunostaining. The nuclei were marked in blue with DAPI. **<0.01 for irradiated versus non-irradiated WT mice. Scale bars, 50 μm.

Histological examination demonstrated that while *K-Tfam*^{+/+} mice at 12 weeks after irradiation presented moderate hyperplasia and no papillomatosis, *K-Tfam*^{-/-} mice presented a papillomatous epidermal hyperplasia, hyperkeratosis showing crusts and parakeratosis, and no dermal invasion. Twenty-five weeks after irradiation, while *K-Tfam*^{+/+} mice presented typical small cell invasive and moderately differentiated SCC, *K-Tfam*^{-/-} presented papillomatous hyperplasia and hyperkeratosis with parakeratosis, without dermal invasion (Figure 5C).

Because DHODH is a key player in the pyrimidine *de novo* biosynthesis pathway, we wondered whether DHODH inhibition and *Tfam* ablation might affect DNA repair efficiency. To confirm this hypothesis, the level of cyclopyrimidine dimer (CPD) was first quantified by immuno-dot blot in DNA of the different groups of mice irradiated for 12 weeks. The CPD level was much higher in leflunomide-treated and *K-Tfam*^{-/-} mice than in *K-Tfam*^{+/+} mice (Figure 6H). Quantification of CPD in the genome of mice by HPLC-MS/MS revealed that the CPD level was respectively 1.82- and 1.74-fold higher in leflunomide-treated and *K-Tfam*^{-/-}

mice than in *K-Tfam*^{+/+} mice (Figure 6I). We then measured the DNA repair capacity of skin mouse samples. To this end, we added the skin protein extracts on a fixed plasmid harboring a defined quantity of CPD. In this assay, the capacity of CPD excision and the re-synthesis of the excised strand is directly correlated with the incorporation of labeled nucleotides. Results indicated a 40% and 54% reduction in CPD repair in leflunomide-treated and *K-Tfam*^{-/-} mice, respectively, as compared with *K-Tfam*^{+/+} mice (Figure 6J).

Because UVB-induced apoptosis is a key determinant affecting the ultimate fate of cells with damaged DNA (Lagerwerf et al., 2011; Surova and Zhivotovsky, 2013), we evaluated the effect of *Tfam* ablation on apoptosis. Western blotting revealed that chronic UVB exposure of *Tfam*^{-/-} mice resulted in an imbalance between proapoptotic (BAX and BAD) and antiapoptotic (BCL-XL and BCL-2) proteins in favor of the former, leading to induction of apoptosis (Figure 6K). Consistently, increased cleaved caspase-3 level (Figures 6K and 6L) and higher caspase-3 activity were found in UVB-irradiated *K-Tfam*^{-/-} mice (Figure 6M). We next examined the effect of *Tfam* ablation on cell-cycle progression. Western blotting revealed that the positive cell-cycle regulators, namely CDK4, CDK6, CDC25C, cyclin B, cyclin D1, and cyclin E were upregulated upon irradiation, and their expressions were higher in *K-Tfam*^{+/+} mice than in *K-Tfam*^{-/-} mice (Figure S4A). The negative cell-cycle regulators, namely p16 and p21^{WAF1}, were increased upon irradiation more pronouncedly in *K-Tfam*^{-/-} mice than in *K-Tfam*^{+/+} mice. Higher levels of phosphorylated ataxia telangiectasia-mutated and Rad3-related (ATR) and phosphorylated CHK1 in irradiated *K-Tfam*^{-/-} mice compared

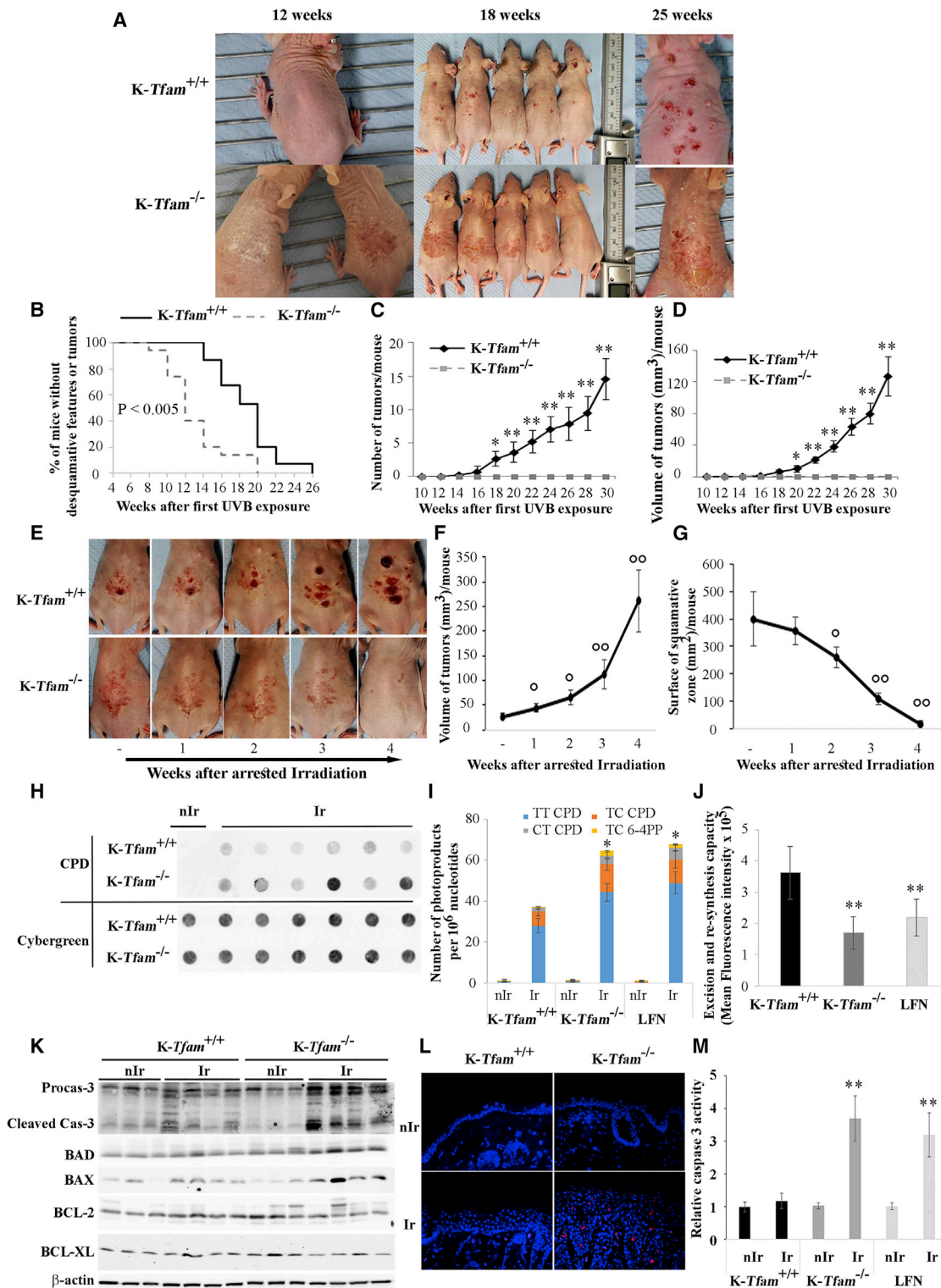


Figure 6. A Keratinocyte-Specific Knockout of *Tfam* Results in Early UVB Exposure Phenotype without Tumor Formation

(A–D) *Tfam*-ablated mice (*K-Tfam*^{-/-}) and their control counterparts (*K-Tfam*^{+/+}) were subjected to chronic UVB irradiation. On *K-Tfam*^{+/+} mice, variable numbers of tumors of variable size that are mostly ulcerated are visible. Some mild pigmentation of UV treated areas is also observed on some mice. The backs of *K-Tfam*^{-/-} mice are covered by a large squame with evidence of peripheral desquamation and there is also evidence of punctiform or larger erosions in the larger

(legend continued on next page)

with irradiated *K-Tfam*^{+/+} mice (Figure S4A) suggested that decreased DNA repair efficiency and subsequently accumulation of DNA damage in *Tfam*-ablated mice possibly delayed the cell-cycle progression and caused increased apoptotic cell death. In line with this hypothesis, colony formation assay, in which the number and size of colonies reflect growth potential of cells, revealed lower proliferation potential of keratinocytes in irradiated *Tfam*^{-/-} compared to *Tfam*^{+/+} (Figures S4B and S4C). To further determine whether the observed hypersensitivity to UVB in *Tfam*-ablated mice is fully dependent on TFAM-DHODH activity-pyrimidine biosynthesis axis, *K-Tfam*^{-/-} mice were received i.p. injection of exogenous uridine (100 mg/kg/day). Assessment of proliferation potential of keratinocytes (Figures S4B and S4C), tumor development (Figures S4D–S4F), CPD quantity (Figure S4G), and apoptosis level (Figure S4H) revealed that pyrimidine supplementation largely reversed the observed hypersensitivity to UVB in *Tfam*-ablated mice.

Altogether, these results strongly suggest that the paradoxical absence of tumor formation in *Tfam*-ablated mice despite the early aggressive UVB exposure phenotype could be related to the decreased pyrimidine biosynthesis and subsequently decreased DNA repair capacity and increased apoptotic cell death.

DHODH Upregulation Persists at Different Stages of Skin Carcinogenesis

We next studied the expression and the activity of DHODH at different stages of carcinogenesis. DHODH was upregulated at a very early phase of UVB-induced tumorigenesis (i.e., hyperplasia), and this upregulation persisted during the subsequent steps of carcinogenesis (Figures 7A and 7B).

We finally investigated DHODH expression and activity in human skin at different stages of carcinogenesis. To this end, we first evaluated the expression of DHODH in skin specimens from healthy individuals, hyperplasia, AK, Bowen's disease, and invasive SCC (Figures 7C and 7D). Immunostaining showed that DHODH was mainly expressed in the basal layer of the epidermis in healthy skin. However, epidermal hyperplasia, AK, Bowen's disease, and invasive SCC specimens displayed diffuse cytoplasmic staining. Of note, the basal keratinocytes in hyperplasia and AK had a higher expression of DHODH compared with other keratinocytes in these specimens. We then assessed the activity of DHODH in skin specimens from healthy individuals, AK, peri-tumoral skin, Bowen's disease, and invasive SCC. Results showed that DHODH activity was

higher in the different stages of carcinogenesis compared to healthy skin (Figure 7E).

DISCUSSION

This study provides insights into the understanding of UVB-induced skin cancer and emphasizes the pivotal role of energy metabolism. We demonstrate that UVB-induced DHODH activation and reductive glutamine metabolism both participate in maintaining nucleotide biosynthesis and cell proliferation, thus paradoxically favoring the development of SCCs. Our data clearly show that LFN-treated mice and TFAM-deficient mice manifest a specific type of hypersensitivity to UVB. However, these mice develop neither actinic keratosis nor skin tumors, even after cessation of UV exposure. Beyond the basic understanding of UVB-induced tumor formation, our findings have substantial implications for the development of new therapeutics for precancerous lesions and established skin cancers, SCC type.

In addition to contributing to amino acid and lipid biosynthesis, mitochondrial metabolism affects nucleotide biosynthesis. Indeed, many components that contribute to both pyrimidine and purine bases are derived directly or indirectly from mitochondria. Besides glutamine and aspartate, which can be supplied by mitochondria, pyrimidine synthesis requires the activity of the mitochondrial enzyme DHODH, linking cellular respiration and pyrimidine synthesis directly (Ahn and Metallo, 2015). In support of this notion, our results indicate that oxygen consumption rate, reductive glutamine metabolism, pyrimidine synthesis, and efficient repair of DNA damage are all dependent on DHODH activity in irradiated skin (see Figures 4L–4N, 6, and S2A–S2C). While respiration is thought to primarily support ATP production and regeneration of electron acceptors (e.g., NAD⁺ and FAD⁺) (Sullivan et al., 2015; Titov et al., 2016), appearance of tumors and rescue of hypersensitivity to UVB in *Tfam*-ablated mice upon uridine supplementation revealed that respiration is specifically required for nucleotide biosynthesis upon irradiation, highlighting a distinct anabolic role for respiration in this condition. Consistently, it has been shown that pyrimidine nucleotide levels are increased in cells in response to other genotoxic stressors such as chemotherapy agents. This upregulation of pyrimidine biosynthesis could be considered as a metabolic vulnerability that can be exploited to enhance the efficacy of chemotherapy and to decrease emergence of resistance, as recently proposed for using doxorubicin and LFN as a promising combination therapy in breast cancer (Brown et al., 2017).

squamous lesions. Mild erythema and pigmentation are also observed on squamous areas (A). The number of mice harboring desquamative features or tumors (B), the number (C), and the volume (D) of tumors per mouse were assessed (mean ± SD) at indicated times.

(E–G) At week 20, chronic UVB exposure was stopped and mice were monitored for one more month (E). While tumors grew on *K-Tfam*^{+/+} (F), hyperkeratic plaques were restored and no tumors were detected on *K-Tfam*^{-/-} mice (G). O p < 0.05 and OO p < 0.005 for indicated time points versus stopped irradiation state (i.e., the first point).

(H and I) Immuno-dot blot (H) and HPLC-MS/MS (I) analysis indicate that the quantity of cyclopyrimidine dimer (CPD) is higher in skin samples of *Tfam*-ablated mice and LFN-treated mice upon chronic UVB irradiation than in control mice.

(J) The capacity of CPD excision and the re-synthesis is lower in *Tfam*-ablated or LFN-treated mice than in control mice.

(K–M) Assessment of protein expression level of pro- and antiapoptotic proteins by western blotting (K), cleaved caspase-3 expression (L), and caspase-3 activity indicates increased apoptotic cell death induction in irradiated *K-Tfam*^{-/-} mice compared with control counterparts (M)

Results are presented as means ± SD. N = 15 (A–D) and (H–K) and 6 (E–G) mice per group. *p < 0.05 and ** < 0.01 for irradiated *K-Tfam*^{-/-} versus irradiated *K-Tfam*^{+/+} mice at corresponding time points. O p < 0.05 and OO p < 0.005 for indicated time points versus stopped irradiation state (i.e., the first point).

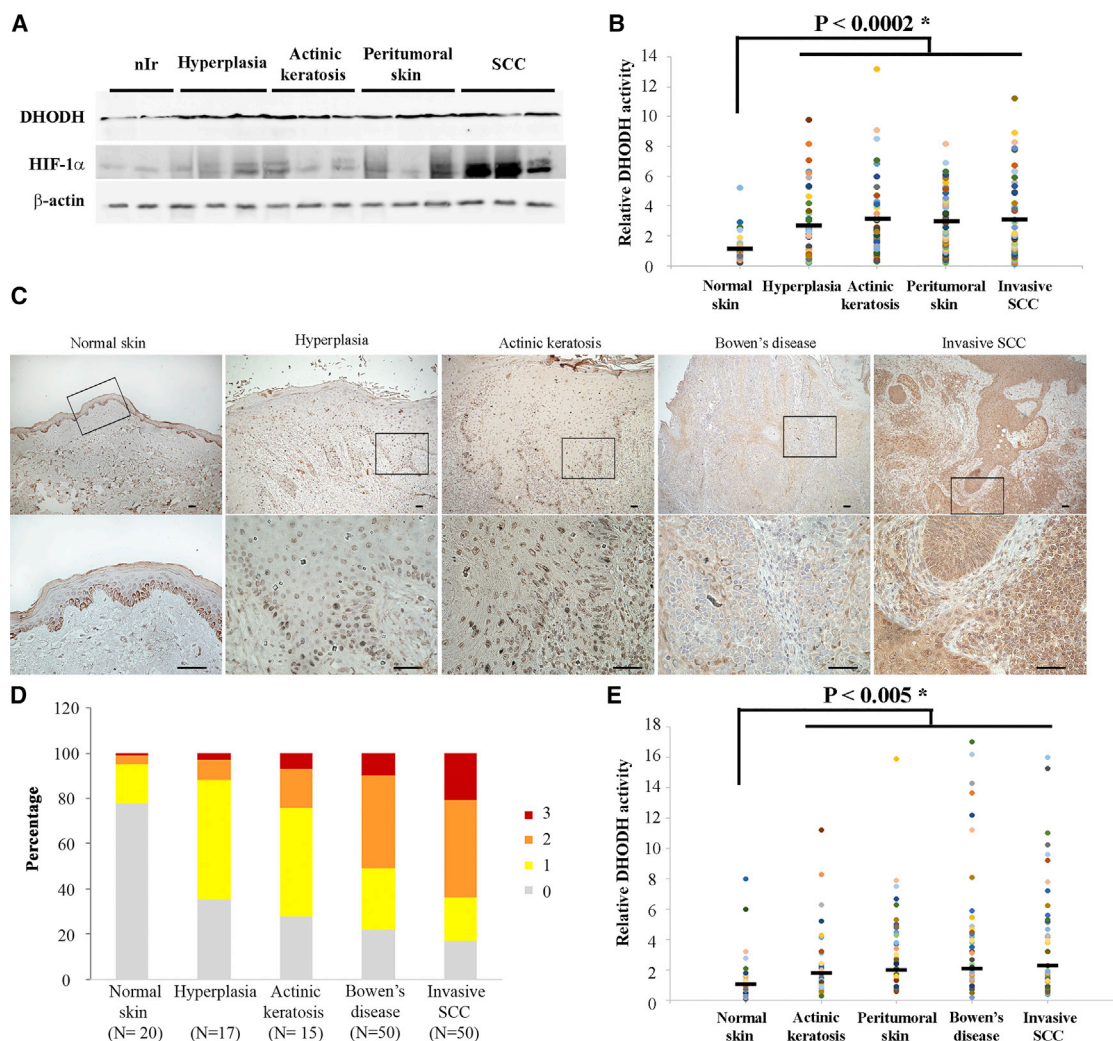


Figure 7. DHODH Upregulation Persists at Different Stages of Skin Carcinogenesis

(A and B) The expression and the activity of DHODH were assessed in mouse skin specimens at different stages of tumorigenesis. Upregulation of DHODH expression (A) and its activity (B) persists at different stages of UVB-induced carcinogenesis. The mean value of DHODH activity in non-irradiated skin samples was set at 1. The results were then compared with this point. Each point corresponds to an individual sample and bars indicate mean values (N = 50 samples per group).

(C and D) DHODH expression was assessed in human skin specimens at different stages of tumorigenesis. Scale bars, 50 μ m (C). Graph shows quantification of DHODH staining intensity (0 = no staining to 3 = high staining) in skin sections excluding the basal layer cells (D).

(E) DHODH activity was evaluated in human skin specimens. The mean value of DHODH activity in normal human skin was arbitrarily set at 1. The results were then compared with this point. Each point corresponds to an individual sample, and bars indicate mean values (N= 50 samples per group).

Reprogramming of the metabolic network is now considered to be a hallmark of neoplastic transformation (Hanahan and Weinberg, 2011). However, altered expressions of metabolic genes are very heterogeneous across different tumor types in that there is no uniform metabolic variation associated with all tumors (Hu et al., 2013). Accumulating evidence indicates that malignant transformation is associated with changes that affect several branches of metabolism to support, on the one hand, the energy demands of cancer cells and, on the other, the anaplerotic reactions that are ultimately required for the generation of sufficient building blocks (i.e., nucleic acids, proteins, and membranes) (Galluzzi et al., 2013; Smolková et al., 2011; Ward

and Thompson, 2012). Here, we show that reprogramming of the energy metabolism could occur during the initial phase of carcinogenesis to support keratinocyte responses to UVB irradiation. Some metabolic modifications including DHODH activation, which occur at a very early phase of UVB-induced tumorigenesis (i.e., hyperplasia), persist during the subsequent steps of carcinogenesis (Figures 1B, 1E, and 7) probably owing to the need for supporting energy demands and anaplerotic reactions of keratinocytes. On the other hand, some other metabolic changes found at the initial phase of carcinogenesis, such as downregulation of glycolysis and upregulation of lipid biosynthesis, can remodel in the final stage of carcinogenesis

(Figures 1B and 1E) possibly owing to the inactivation of a tumor suppressor gene, activation of an oncogene, and/or adaptation to the tumor microenvironment. In support to the first notion, inactivated DHODH or impaired ETC blocks neoplastic transformation of keratinocytes. Consistent with our results, treatment of mice with metformin, which interrupts the mitochondrial respiratory chain at complex I, resulted in the significant delayed onset of UVB- and chemical-induced skin tumorigenesis and the reduced tumor multiplicity (Checkley et al., 2014; Wu et al., 2013). Growth of UVB-induced established tumors has also been shown to be slowed down following treatment with metformin (Wu et al., 2013). In addition, upregulation and overactivation of DHODH have been reported in several types of cancers (Ahn and Metallo, 2015; He et al., 2014; Hu et al., 2013; White et al., 2011; Zhai et al., 2013). In accordance, inhibition of DHODH or knockout of *Tfam* have been demonstrated to reduce tumor growth (Weinberg et al., 2010; White et al., 2011; Zhai et al., 2013). In support of the second notion, increased expression of enzymes involved in glycolysis in SCC could be related to the overexpression of hypoxia inducible factor (HIF)-1 α (Figure 7A).

Altogether, our findings highlight the dynamic role of mitochondria in the regulation of UVB-induced carcinogenesis. Our results also suggest that modifications in energy metabolism can be exploited for skin tumor prevention and curative treatment.

EXPERIMENTAL PROCEDURES

Animals and Experimental Protocol

SKH-1 hairless mice were purchased at 4–6 weeks of age from Charles River (L'arles, France). *Tfam*^{flox/flox} mice were kindly provided by Dr. Nils-Göran Larsson, Max Planck Institute for Biology of Aging, Cologne Germany. K14-Cre-ER^{T2} mice expressing inducible Cre recombinase under the control of the keratinocyte-specific K14 promoter (K14-Cre) were purchased from Jackson Laboratory. Hairless *Tfam*^{flox/flox} mice and Hairless K14-Cre-ER^{T2} mice were generated by cross-breeding with hairless SKH-1 mice for 5 generations. The progeny was genotyped by PCR assays on tail DNA. Crossing these strains then generated the K14-Cre-ER^{T2}/*Tfam*^{flox/flox}. Mice in which TFAM deficiency was restricted to keratinocytes were then generated by topical skin application of 4-hydroxytamoxifen (OHT) at 1 mg kg⁻¹ for 5 consecutive days. *Tfam* ablation in keratinocytes was verified by PCR assays on skin DNA (Figure S5). Mice were bred and maintained in a pathogen-free mouse facility. All mouse experiments were carried out with the approval of Bordeaux University Animal Care and Use Committee. In all experiments, female mice were used. Mice were randomly assigned to each group before the start and experiments were performed blinded with respect to genotype and/or treatment. Chronic irradiation was started at age 7–9 weeks.

Cellular O₂/CO₂ Exchange

A Seahorse XF24 Extracellular Flux Analyzer (Seahorse Bioscience) was used to analyze the bioenergetic function of skin samples. Results were normalized with weight of skin samples for potential differences in skin size. Slices on nylon inserts were individually inserted face down into 20 wells of 24-well XF Islet Capture Microplates that contained 500 μ L of assay medium. The assay medium for measurement of glycolytic capacity was XF Base medium (Sigma) supplemented with penicillin (100 IU/mL) and streptomycin (100 μ g/mL) adjusted to pH 7.4. The assay medium for measurement of OXPHOS capacity consisted in XF Base medium supplemented with D-glucose (11 mM), sodium pyruvate (1 mM), penicillin (100 IU/mL), and streptomycin (100 μ g/mL) adjusted to pH 7.4 for measurement of OCR or ECAR. For fatty acid β -oxidation, skin samples were put in a modified Krebs-Henseleit-bicarbonate buffer (KHB) supplemented with 2.5 mM glucose, 50 μ M carnitine, and 5 mM HEPES

adjusted to pH 7.4. Four wells contained inserts but no skin samples to control for temperature-sensitive fluctuations in O₂ fluorophore emission. Once the transfer of inserts was complete, samples in XF Islet Capture Microplates were incubated in a CO₂-free incubator at 37°C for 1 hr to allow temperature and pH equilibration. Microplates were then put into XF24 and allowed to equilibrate for 15 min prior to first measurement. XF assays consisted of 3 min mix, 3 min wait, and 2 min measurement cycles and were performed at 37°C as described elsewhere (Wu et al., 2007). Using this protocol, it was possible to calculate an O₂ consumption rate every 8 min. Drugs of interest prepared in the requisite assay medium (75 μ L) were preloaded into reagent delivery chambers A, B, C, and D at 10 \times , 11 \times , 12 \times , and 13 \times the final working concentration, respectively, and injected sequentially at intervals of 24 min as indicated. The substrates were added as indicated in the figures at the following final working concentrations: oligomycin (25 μ M), rotenone (25 μ M), antimycin A (50 μ M), digitonin (4 μ M), succinate (25 mM), DNP (100 μ M), dihydroorotic acid (10 mM), and etomoxir (200 μ M). The optimal concentration of drugs and skin size was determined following titration assays (Table S3). In each 24-well plate, both non-irradiated and irradiated samples were put in triplicate. The consumption of oxygen by irradiated samples were then compared with those of non-irradiated skin in the same plate by setting the consumption of oxygen by non-irradiated skin in each plate to 100%.

Proteomic Analysis

Sample preparation, nano-scale liquid chromatographic tandem mass spectrometry analysis, database search, processing of results, and label-free quantitative data analysis are detailed in the Supplemental Information.

Statistics

Comparisons between two groups were calculated using Student's t test (two tailed) and a p value < 0.05 (*) was considered significant. Results are presented as means \pm SD. Comparisons between more than two groups were calculated with one-way ANOVA followed by Bonferroni's multiple comparison tests. To assess the OCR data, the number and the volume of tumors, two-way ANOVA followed by a post hoc Tukey's test was used. A p value < 0.05 (*) was considered significant. Results are presented as means \pm SD.

SUPPLEMENTAL INFORMATION

Supplemental Information includes Supplemental Experimental Procedures, five figures, and three tables and can be found with this article online at <https://doi.org/10.1016/j.celrep.2018.05.060>.

ACKNOWLEDGMENTS

The authors wish to thank P. Costet (University of Bordeaux) and Véronique Guyonnet-Duperat (FR TransBioMed, Plateforme de Vectorologie, University of Bordeaux) and Prof. Nils-Göran Larsson and Dr. Bettina Bertalan (Max Planck Institute for Biology of Ageing/Animal Facility, Cologne, Germany) for their valuable expertise and sharing the *Tfam*^{flox/flox} mice. The authors acknowledge Vanessa Bergeron and Doriane Bortolotto for technical help and Pr. Hubert de Verneuil for useful discussion. H.R.R. gratefully acknowledges support from the ARC "Association pour la Recherche sur le Cancer," the Institut National du Cancer "INCA_6654," INCa-Canceropôle GSO, and FR TransBioMed. A.-K.B.-S. is supported by the Labex TRAIL (ANR-10-LABX-57). L.D. was supported by a grant from the SFD "Société Française de Dermatologie".

AUTHOR CONTRIBUTIONS

M.H. and L.D. designed and performed the experiments and analyzed the data. R.R., A.-K.B.-S., M.V., and Z.I. performed some experiments, analyzed the data, and provided constructive comments. W.M. and M.S.-S. helped to generate transgenic mice and performed chronic irradiation. I.R.-V., S.M., Z.K., E.O., W.R., and T.D. performed some experiments. M.B. and S.C. performed the proteomic procedure. A.T. analyzed some of the data and provided constructive comments on the paper. H.R.R. designed the experiments, analyzed the data, and wrote the paper.

DECLARATION OF INTERESTS

None of the authors has any financial interest related to this work. A patent is pending on the biomarkers for different stage of skin carcinogenesis with H.R.R., M.H., and R.R. as inventors and Bordeaux University as owner of the patent.

Received: December 24, 2015

Revised: April 5, 2018

Accepted: May 17, 2018

Published: June 19, 2018

REFERENCES

- Ahn, C.S., and Metallo, C.M. (2015). Mitochondria as biosynthetic factories for cancer proliferation. *Cancer Metab.* 3, 1.
- Baris, O.R., Klose, A., Kloepper, J.E., Weiland, D., Neuhaus, J.F., Schauen, M., Wille, A., Müller, A., Merkwirth, C., Langer, T., et al. (2011). The mitochondrial electron transport chain is dispensable for proliferation and differentiation of epidermal progenitor cells. *Stem Cells* 29, 1459–1468.
- Branzei, D., and Foiani, M. (2008). Regulation of DNA repair throughout the cell cycle. *Nat. Rev. Mol. Cell Biol.* 9, 297–308.
- Brown, K.K., Spinelli, J.B., Asara, J.M., and Toker, A. (2017). Adaptive reprogramming of *de novo* pyrimidine synthesis is a metabolic vulnerability in triple-negative breast cancer. *Cancer Discov.* 7, 391–399.
- Campbell, C.T., Kolesar, J.E., and Kaufman, B.A. (2012). Mitochondrial transcription factor A regulates mitochondrial transcription initiation, DNA packaging, and genome copy number. *Biochim. Biophys. Acta* 1819, 921–929.
- Caro, P., Kishan, A.U., Norberg, E., Stanley, I.A., Chapuy, B., Ficarro, S.B., Polak, K., Tondera, D., Gounarides, J., Yin, H., et al. (2012). Metabolic signatures uncover distinct targets in molecular subsets of diffuse large B cell lymphoma. *Cancer Cell* 22, 547–560.
- Checkley, L.A., Rho, O., Angel, J.M., Cho, J., Blando, J., Beltran, L., Hursting, S.D., and DiGiovanni, J. (2014). Metformin inhibits skin tumor promotion in overweight and obese mice. *Cancer Prev. Res. (Phila.)* 7, 54–64.
- DiGiovanni, J. (1992). Multistage carcinogenesis in mouse skin. *Pharmacol. Ther.* 54, 63–128.
- Emadi, A., Jun, S.A., Tsukamoto, T., Fathi, A.T., Minden, M.D., and Dang, C.V. (2014). Inhibition of glutaminase selectively suppresses the growth of primary acute myeloid leukemia cells with IDH mutations. *Exp. Hematol.* 42, 247–251.
- Galluzzi, L., Kepp, O., Vander Heiden, M.G., and Kroemer, G. (2013). Metabolic targets for cancer therapy. *Nat. Rev. Drug Discov.* 12, 829–846.
- Hamanaka, R.B., Glasauer, A., Hoover, P., Yang, S., Blatt, H., Mullen, A.R., Getsios, S., Gottardi, C.J., DeBerardinis, R.J., Lavker, R.M., and Chandel, N.S. (2013). Mitochondrial reactive oxygen species promote epidermal differentiation and hair follicle development. *Sci. Signal.* 6, ra8.
- Hanahan, D., and Weinberg, R.A. (2011). Hallmarks of cancer: the next generation. *Cell* 144, 646–674.
- He, T., Haapa-Paananen, S., Kaminsky, V.O., Kohonen, P., Fey, V., Zhivotovskiy, B., Kallioniemi, O., and Perälä, M. (2014). Inhibition of the mitochondrial pyrimidine biosynthesis enzyme dihydroorotate dehydrogenase by doxorubicin and brequinar sensitizes cancer cells to TRAIL-induced apoptosis. *Oncogene* 33, 3538–3549.
- Hosseini, M., Kasraian, Z., and Rezvani, H.R. (2017). Energy metabolism in skin cancers: A therapeutic perspective. *Biochim. Biophys. Acta* 1858, 712–722.
- Hu, J., Locasale, J.W., Bielas, J.H., O'Sullivan, J., Sheahan, K., Cantley, L.C., Vander Heiden, M.G., and Vitkup, D. (2013). Heterogeneity of tumor-induced gene expression changes in the human metabolic network. *Nat. Biotechnol.* 31, 522–529.
- Jose, C., Bellance, N., and Rossignol, R. (2011). Choosing between glycolysis and oxidative phosphorylation: a tumor's dilemma? *Biochim. Biophys. Acta* 1807, 552–561.
- Kang, D., Kim, S.H., and Hamasaki, N. (2007). Mitochondrial transcription factor A (TFAM): roles in maintenance of mtDNA and cellular functions. *Mitochondrion* 7, 39–44.
- Lagerwerf, S., Vrouwe, M.G., Overmeer, R.M., Fouteri, M.I., and Mullenders, L.H. (2011). DNA damage response and transcription. *DNA Repair (Amst.)* 10, 743–750.
- Liberti, M.V., and Locasale, J.W. (2016). The Warburg effect: how does it benefit cancer cells? *Trends Biochem. Sci.* 41, 211–218.
- Obre, E., and Rossignol, R. (2015). Emerging concepts in bioenergetics and cancer research: metabolic flexibility, coupling, symbiosis, switch, oxidative tumors, metabolic remodeling, signaling and bioenergetic therapy. *Int. J. Biochem. Cell Biol.* 59, 167–181.
- Pavlova, N.N., and Thompson, C.B. (2016). The emerging hallmarks of cancer metabolism. *Cell Metab.* 23, 27–47.
- Porporato, P.E., Payen, V.L., Pérez-Escuredo, J., De Saedeleer, C.J., Danhier, P., Copetti, T., Dhup, S., Tardy, M., Vazeille, T., Bouzin, C., et al. (2014). A mitochondrial switch promotes tumor metastasis. *Cell Rep.* 8, 754–766.
- Rogers, H.W., Weinstock, M.A., Feldman, S.R., and Coldiron, B.M. (2015). Incidence estimate of nonmelanoma skin cancer (keratinocyte carcinomas) in the US population, 2012. *JAMA* 314, 1081–1086.
- Seltzer, M.J., Bennett, B.D., Joshi, A.D., Gao, P., Thomas, A.G., Ferraris, D.V., Tsukamoto, T., Rojas, C.J., Slusher, B.S., Rabinowitz, J.D., et al. (2010). Inhibition of glutaminase preferentially slows growth of glioma cells with mutant IDH1. *Cancer Res.* 70, 8981–8987.
- Smolková, K., Plecítá-Hlavatá, L., Bellance, N., Benard, G., Rossignol, R., and Ježek, P. (2011). Waves of gene regulation suppress and then restore oxidative phosphorylation in cancer cells. *Int. J. Biochem. Cell Biol.* 43, 950–968.
- Sullivan, L.B., Gui, D.Y., Hosios, A.M., Bush, L.N., Freinkman, E., and Vander Heiden, M.G. (2015). Supporting aspartate biosynthesis is an essential function of respiration in proliferating cells. *Cell* 162, 552–563.
- Surova, O., and Zhivotovskiy, B. (2013). Various modes of cell death induced by DNA damage. *Oncogene* 32, 3789–3797.
- Titov, D.V., Cracan, V., Goodman, R.P., Peng, J., Grabarek, Z., and Mootha, V.K. (2016). Complementation of mitochondrial electron transport chain by manipulation of the NAD⁺/NADH ratio. *Science* 352, 231–235.
- Vander Heiden, M.G., Cantley, L.C., and Thompson, C.B. (2009). Understanding the Warburg effect: the metabolic requirements of cell proliferation. *Science* 324, 1029–1033.
- Villar, V.H., Merhi, F., Djavaheri-Mergny, M., and Duran, R.V. (2015). Glutaminolysis and autophagy in cancer. *Autophagy* 11, 1198–1208.
- Ward, P.S., and Thompson, C.B. (2012). Metabolic reprogramming: a cancer hallmark even warburg did not anticipate. *Cancer Cell* 21, 297–308.
- Weinberg, F., Hamanaka, R., Wheaton, W.W., Weinberg, S., Joseph, J., Lopez, M., Kalyanaraman, B., Mutlu, G.M., Budinger, G.R., and Chandel, N.S. (2010). Mitochondrial metabolism and ROS generation are essential for Kras-mediated tumorigenicity. *Proc. Natl. Acad. Sci. USA* 107, 8788–8793.
- White, R.M., Cech, J., Ratanasirintrao, S., Lin, C.Y., Rahl, P.B., Burke, C.J., Langdon, E., Tomlinson, M.L., Mosher, J., Kaufman, C., et al. (2011). DHODH modulates transcriptional elongation in the neural crest and melanoma. *Nature* 471, 518–522.
- Wu, M., Neilson, A., Swift, A.L., Moran, R., Tamagnine, J., Parslow, D., Armistead, S., Lemire, K., Orrell, J., Teich, J., et al. (2007). Multiparameter metabolic analysis reveals a close link between attenuated mitochondrial bioenergetic function and enhanced glycolysis dependency in human tumor cells. *Am. J. Physiol. Cell Physiol.* 292, C125–C136.
- Wu, C.L., Qiang, L., Han, W., Ming, M., Viollet, B., and He, Y.Y. (2013). Role of AMPK in UVB-induced DNA damage repair and growth control. *Oncogene* 32, 2682–2689.
- Zhai, H., Song, B., Xu, X., Zhu, W., and Ju, J. (2013). Inhibition of autophagy and tumor growth in colon cancer by miR-502. *Oncogene* 32, 1570–1579.
- Zong, W.X., Rabinowitz, J.D., and White, E. (2016). Mitochondria and cancer. *Mol. Cell* 61, 667–676.